Eur. Phys. J. A (2014) **50**: 4
DOI 10.1140/epja/i2014-14004-3

THE EUROPEAN PHYSICAL JOURNAL A

Regular Article – Experimental Physics

Elastic and inelastic scattering of $^{14}C + ^{11}B$ versus $^{12,13}C + ^{11}B$

S.Yu. Mezhevych[1], A.T. Rudchik[1,a], K. Rusek[2,7], K.W. Kemper[3], S. Kliczewski[4], E.I. Koshchy[5], A.A. Rudchik[1], S.B. Sakuta[6], J. Choiński[7], B. Czech[4], R. Siudak[4], and A. Szczurek[4]

[1] Institute for Nuclear Research, Prospekt Nauky 47, 03680 Kyiv, Ukraine
[2] National Institute for Nuclear Research, ul. Hoża 69, PL-00-681 Warsaw, Poland
[3] Physics Department, Florida State University, Tallahassee, Florida 32306-4350, USA
[4] H. Niewodniczański Institute of Nuclear Physics, ul. Radzikowskiego 152, PL-31-342 Cracow, Poland
[5] Kharkiv National University, pl. Svobody 4, 61077 Kharkiv, Ukraine
[6] Russian Research Center "Kurchatov Institute", 123182 Moscow, Russia
[7] Heavy Ion Laboratory of Warsaw University, ul. L. Pasteura 5A, PL-02-093 Warsaw, Poland

Received: 24 July 2013 / Revised: 19 December 2013
Published online: 22 January 2014 –
Communicated by N. Kalantar-Nayestanaki

Abstract. Complete angular distributions of the $^{14}C + ^{11}B$ elastic and inelastic scattering at the energy $E_{lab}(^{11}B) = 45$ MeV were measured for the ground and excited states of ^{11}B. The data were analyzed within the optical model and the coupled-reaction-channels method. The parameters of the $^{14}C + ^{11}B$ optical potential and ^{11}B deformation were deduced. The contributions of one- and two-step transfers of nucleons and clusters into the $^{14}C + ^{11}B$ elastic and inelastic scattering were calculated. The isotopic differences between the $^{14}C + ^{11}B$ and $^{12,13}C + ^{11}B$ scatterings are presented and clearly show the importance of the large angle scattering data for understanding the interaction between light heavy ions.

1 Introduction

An early paper of J.S. Blair [1] predicted that effects arising from the internal structure of interacting heavy ions would show up as dramatic differences in the elastic scattering when compared with those observed for the light nuclei ^{4,3}He and t, d and p. One prediction was that there would be contributions to the elastic scattering from the non-spherical part of the matter distribution of nuclei that had large ground-state quadrupole moments. This prediction was confirmed by scattering ^{10}B, ^{11}B and ^{12}C from ^{27}Al and measuring the elastic scattering as a ratio to Rutherford through four orders of magnitude [2]. Based on the fact that ^{12}C has no ground-state quadrupole moment, ^{11}B has one of 4 fm^2 and ^{10}B 8 fm^2, the ^{12}C elastic scattering was oscillatory at the larger angles, ^{11}B less so and ^{10}B the least oscillator as predicted.

Recently, several papers have been published for scattering of ^{11}B by the carbon isotopes ^{12}C [3] and ^{13}C [4] where in addition to quadrupole effects from the projectile, the role of transfer of a proton or a deuteron or (pn) pair could be studied by measuring data throughout the whole angular range by detecting both the incoming ^{11}B projectile and the carbon recoil. In each case the large angle elastic scattering is much greater than would be expected if the elastic scattering were only determined by potential scattering from a spherical nucleus. For $^{11}B+^{12}C$ elastic scattering, it was found that the observed enhanced large angle elastic scattering arose from contributions from both reorientation of the ^{11}B ground state and from proton transfer between the interacting partners. In $^{11}B+^{13}C$, the large angle scattering was smaller in magnitude than that from ^{12}C and had as its main contributions potential scattering and reorientation of ^{11}B.

A surprising result in the case of $^{11}B+^{12}C$ was the large contribution to the ^{11}B inelastic scattering from proton transfer as was confirmed by the fact that in the case of $^{11}B+^{13}C$ inelastic scattering only inelastic excitations produced the observed cross sections. In the case of $^{11}B+^{14}C$ elastic and inelastic scattering, it would be expected that the large angle scattering would be smaller than that for ^{12}C but its magnitude, when compared to that for scattering from ^{13}C, might be the same since particle transfer channels are less likely between ^{11}B and ^{14}C as these would require larger clusters or groups of nucleons to be transferred to make an impact on the scattering. In a previous work [5], the $^{14}C+^{11}B$ elastic and inelastic scattering data at the energy $E_{lab}(^{11}B) = 45$ MeV were studied only for the excitations of ^{14}C to determine its ground-state shape and the possible halo structure of its excited states.

[a] e-mail: rudchik@kinr.kiev.ua

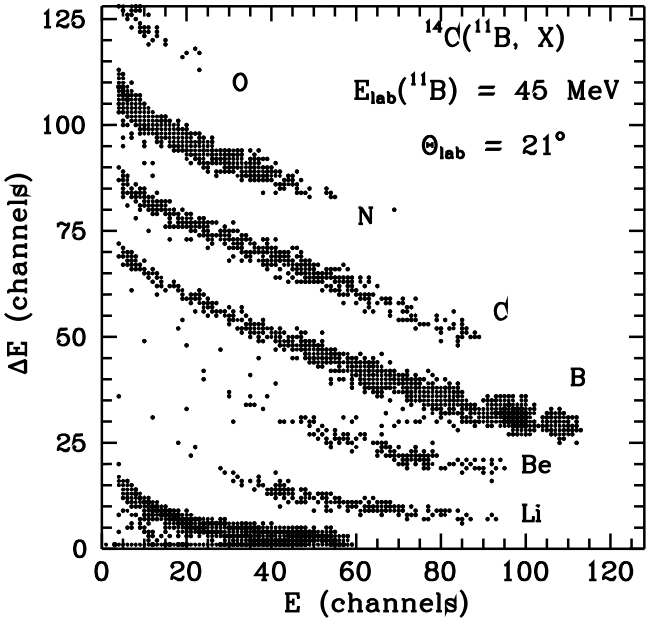

Fig. 1. Typical $\Delta E(E)$-spectrum of the ^{14}C(^{11}B, X) reaction products at the energy $E_{\rm lab}(^{11}{\rm B}) = 45\,{\rm MeV}$.

In the present work the excitations of states in ^{11}B were determined and compared to results for other systems. The $^{14}{\rm C} + ^{11}{\rm B}$ optical potential and deformation parameters of ^{11}B deduced in this work, will be used in coupled-reaction-channels (CRC) calculations to study the simultaneously measured ^{14}C(^{11}B, X)Y reactions and deduce parameters for the $X + Y$ optical potentials, using needed spectroscopic amplitudes for nucleons and clusters which can be calculated within the shell model. To obtain information about the isotopic difference of the $^{12,13,14}{\rm C} + ^{11}{\rm B}$ optical potentials, the $^{14}{\rm C} + ^{11}{\rm B}$ optical potential is compared with $^{12}{\rm C} + ^{11}{\rm B}$ and $^{13}{\rm C} + ^{11}{\rm B}$ potentials obtained previously at the energies $E_{\rm lab}(^{11}{\rm B}) = 49\,{\rm MeV}$ [3] and 45 MeV [4], respectively.

2 Experimental procedure

Angular distributions of the $^{14}{\rm C} + ^{11}{\rm B}$ elastic and inelastic scattering were measured simultaneously with the ^{14}C(^{11}B, X) transfer reactions, using the 45 MeV beam of ^{11}B from the Warsaw University cyclotron. A self-supporting $280\,\mu{\rm g/cm}^2$ foil of carbon enriched to 86% in ^{14}C was used as the target. The beam energy spread on the target did not exceed 0.5%.

The reaction products were detected by a silicon ΔE-E telescope with a $40\,\mu$m silicon ΔE-detector and by two telescopes with an ionization chamber as the ΔE-detector. The three 1 mm silicon E-detectors were used in the telescopes.

The standard CAMAC electronics and computer acquisition system SMAN [6] were used in the present experiment.

A typical $\Delta E(E)$-spectrum of the ^{14}C(^{11}B, X) reaction products measured with the telescope composed of the ionization chamber as a ΔE-detector is presented in fig. 1. As one can see, the reaction products were well resolved only by charge.

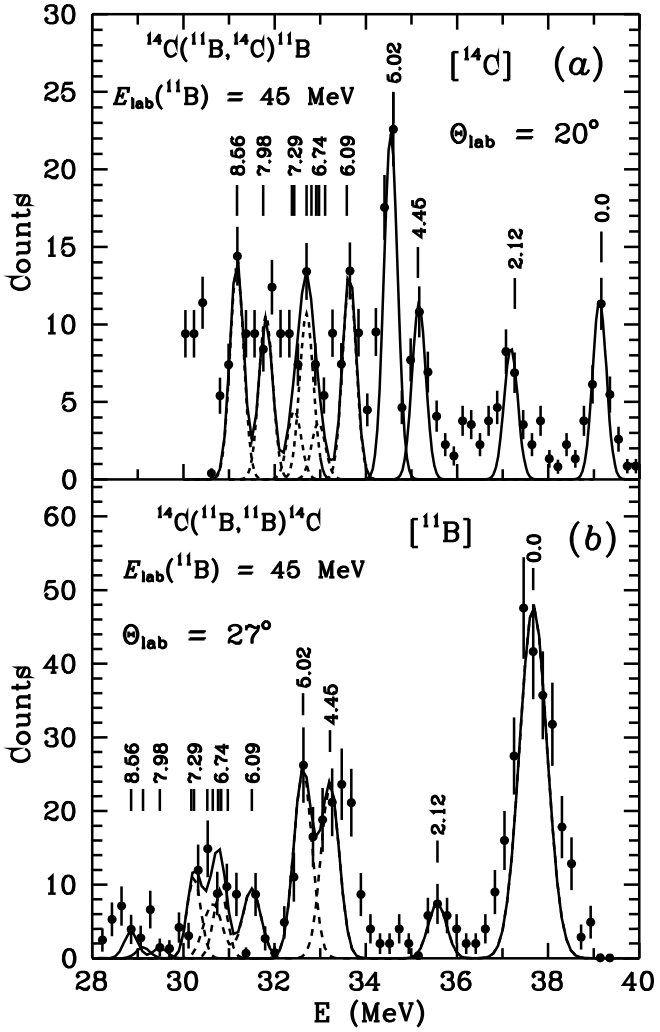

Fig. 2. Typical energy spectra of ^{11}B (a) and ^{14}C (b) nuclei from the ^{14}C(^{11}B, X) reaction at the energy $E_{\rm lab}(^{11}{\rm B}) = 45\,{\rm MeV}$.

Typical residual energy spectra of ^{11}B (a) and ^{14}C (b) after the subtraction of background from multi-particle reactions and the ^{12}C in the target are shown in fig. 2. The curves show the symmetric Gauss functions fit to the spectra peaks. The areas under the peaks of the residual ^{11}B and ^{14}C spectra were used for the calculation of angular distributions at the angles $\theta_{\rm c.m.}(^{11}{\rm B})$ and $\theta_{\rm c.m.}(^{11}{\rm B}) = 180^\circ - \theta_{\rm c.m.}(^{14}{\rm C})$, respectively. In this way, angular distributions for ^{14}C(^{11}B, ^{11}B) scattering over the whole angular range were determined.

The angular distributions of the $^{14}{\rm C} + ^{11}{\rm B}$ elastic scattering were normalized to the OM cross section at small angles where it is relatively independent of nuclear potential parameters. The normalization error was smaller than 15%. The same factor was used to normalize the angular distributions for both elastic- and inelastic-scattering data at the forward and backward angles.

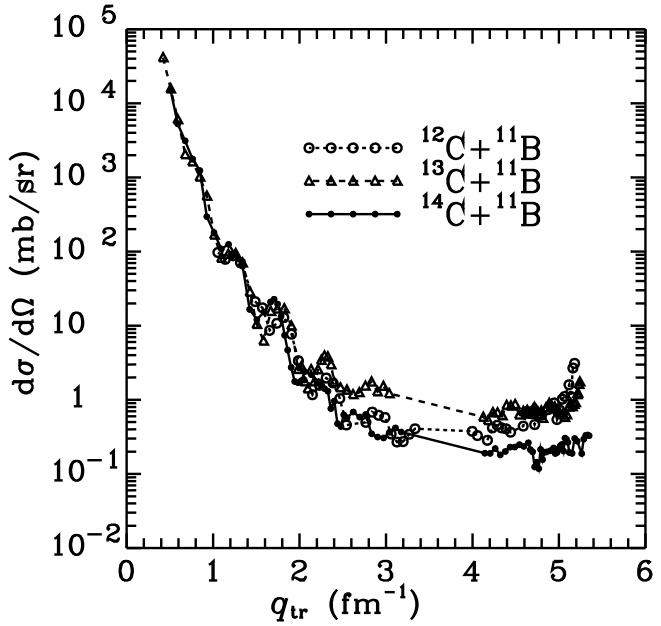

Fig. 3. Momentum transfer distributions q_t of ^{14}C+^{11}B elastic scattering at the energy $E_{\rm lab}(^{11}{\rm B}) = 45\,{\rm MeV}$ (filled symbols) *versus* that of $^{13}{\rm C} + {}^{11}{\rm B}$ at the same energy [4] (triangle symbols) and ^{12}C+^{11}B at $E_{\rm lab}(^{11}{\rm B}) = 49\,{\rm MeV}$ [3] (open symbols).

In fig. 3, the measured distribution of the $^{14}{\rm C} + {}^{11}{\rm B}$ elastic scattering at the energy $E_{\rm lab}(^{11}{\rm B}) = 45\,{\rm MeV}$ (filled symbols) is compared with that of $^{12}{\rm C} + {}^{11}{\rm B}$ distribution at $E_{\rm lab}(^{11}{\rm B}) = 49\,{\rm MeV}$ [3] (open symbols) and $^{13}{\rm C} + {}^{11}{\rm B}$ distribution at $E_{\rm lab}(^{11}{\rm B}) = 45\,{\rm MeV}$ [4] (open triangle symbols) as a function of transferred momentum q_t. One can see that these data agree satisfactorily especially at the smaller transferred momentum q_t, while they differ at $q_t > 2.5\,{\rm fm}^{-1}$ clearly demonstrating differences in the reaction contributions to the scattering at the larger transferred momenta.

3 The data analysis

3.1 Calculation procedure

Optical model (OM) potentials of Woods-Saxon type with volume absorption and parameters $X_i = \{V_0, r_V, a_V, W_S, r_W, a_W\}$ and Coulomb potentials of a uniform charged sphere with parameter $r_C = 1.25\,{\rm fm}$ were used in OM and CRC calculations with the radii given by

$$R_i = r_i(A_P^{1/3} + A_T^{1/3})\ (i = V, W_S, C) \qquad (1)$$

for the scattering of projectile ions (P) by target nuclei (T).

In the CRC analysis, the $^{14}{\rm C} + {}^{11}{\rm B}$ elastic and inelastic scattering for the transitions to the ground and excited states of ^{11}B and ^{14}C, spin reorientation of ^{11}B and most important transfer reactions were included in the channels coupling scheme. Figure 4 shows the transitions to the excited states of ^{11}B and ^{14}C. The diagrams of one- (single-) and two-step transfers, which contribute to the $^{14}{\rm C} + {}^{11}{\rm B}$ scattering calculations, are presented in fig. 5.

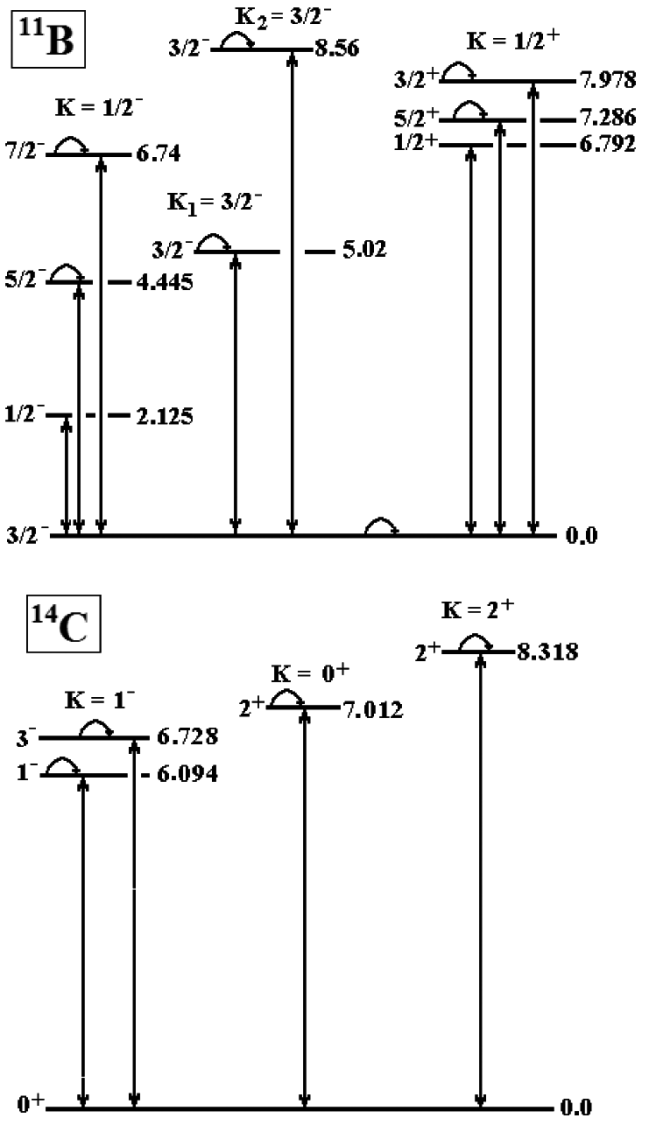

Fig. 4. Coupling schemes for the transitions to the excited states of ^{11}B and ^{14}C. The arcs show the spin reorientations of ^{11}B and ^{14}C in ground and excited states.

We assume that the rotations of the deformed ^{11}B and ^{14}C nuclei as well as vibrations dominate the low-energy excitations. The transitions to these states were calculated using the form factors

$$V_\lambda(r) = -\frac{\delta_\lambda}{\sqrt{4\pi}}\frac{{\rm d}U(r)}{{\rm d}r}, \qquad (2)$$

where δ_λ is the length of the λ-multipole deformation. The values of the deformation parameters δ_λ and $\beta_\lambda = \delta_\lambda/R$ ($R = 1.25\,A^{1/3}$) of ^{11}B and ^{14}C are listed in table 1. The deformation length $\delta_\lambda = 1.2\,{\rm fm}$ found in the inelastic scattering analysis as described in the next section was used in the CRC calculation of the ^{11}B ground-state reorientation.

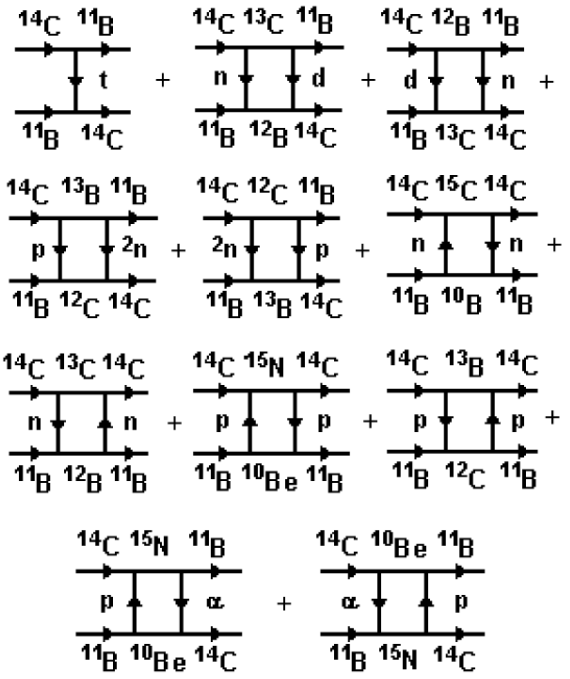

Fig. 5. Diagrams of one- and two-step transfers contributing to the $^{14}\mathrm{C} + {}^{11}\mathrm{B}$ scattering calculations.

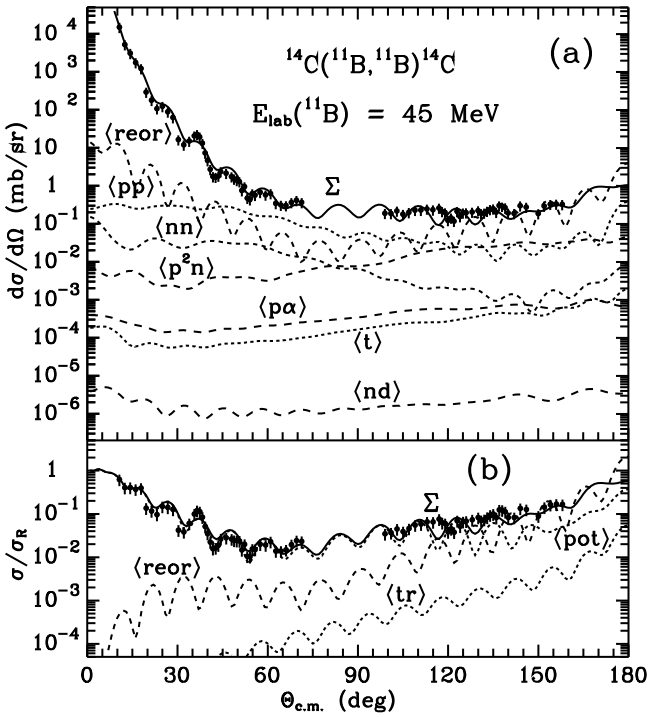

Fig. 6. Angular distributions of the $^{14}\mathrm{C}+{}^{11}\mathrm{B}$ elastic scattering at the energy $E_{\mathrm{lab}}(^{11}\mathrm{B}) = 45\,\mathrm{MeV}$ in absolute units (a) and as relation to the Rutherford scattering (b). The curves show the CRC calculations for different nuclear processes. Σ-curves show the coherent sums of all processes.

Table 1. Deformation parameters of $^{11}\mathrm{B}$ and $^{14}\mathrm{C}$.

Nucleus	E_x (MeV)	J^π	λ	δ_λ (fm)	$\beta_\lambda^{(a)}$	Ref.
^{11}B	2.125	$1/2^-$	2	1.2	0.43	[3]
	4.445	$5/2^-$	2	1.2	0.43	[3]
			4	1.0	0.36	[3]
	5.021	$3/2^-$	2	1.2	0.43	[3]
	6.743	$7/2^-$	2	1.2	0.43	[3]
			4	1.0	0.36	[3]
	6.792	$1/2^+$	1	1.0	0.36	[4]
	7.286	$5/2^+$	1	1.0	0.36	[4]
			3	1.2	0.43	[4]
	7.978	$3/2^+$	1	1.0	0.36	[4]
			3	1.2	0.43	[4]
	8.560	$3/2^-$	2	1.2	0.43	[4]
^{14}C	6.094	1^-	1	0.4	0.13	[5]
	6.728	3^-	3	1.0	0.35	[5]
	7.012	2^+	2	−0.6	−0.2	[5]
	8.318	2^+	2	−0.6	−0.2	[5]

(a) $\beta_\lambda = \delta_\lambda/R$, $R = 1.25\,A^{1/3}$.

The spectroscopic amplitudes S_x of transferred clusters or nucleons x in the $A = C + x$ systems required for the CRC calculations of the transfer reactions were obtained within the translationally invariant shell model (TISM) [7] using code DESNA [8,9]. The amplitudes S_x are listed in table 2.

The wave function of the bound state of cluster x was calculated by fitting the Woods-Saxon potential parameter V to the x-cluster binding energy in the $A = C+x$ system for $a_V = 0.65\,\mathrm{fm}$ and $r_V = 1.25\,A^{1/3}/(C^{1/3}+x^{1/3})\,\mathrm{fm}$. The codes SPI-GENOA [10] and FRESCO [11] were used for the OM and CRC calculations, respectively.

In CRC calculations of $^{14}\mathrm{C}+{}^{11}\mathrm{B}$ scattering, a prior interaction was used. The transfer reactions were calculated in a finite-range approximation with a prior interaction for the single (first)-step transfers and post interaction for the second-step transfers. In both cases, the full real remnants without "non-orthogonality remnants" were used.

The angular distribution of the measured $^{14}\mathrm{C} + {}^{11}\mathrm{B}$ elastic scattering at the energy $E_{\mathrm{lab}}(^{11}\mathrm{B}) = 45\,\mathrm{MeV}$ are presented in fig. 6. First, the data were analyzed within the OM. Next, the deduced optimum potential parameters $X_i = \{V_0, r_V, a_V, W_S, r_W, a_W\}$ were optimized in the CRC calculations. The potential parameters, volume integrals J_V, J_W and root-mean-square radii R_V, R_W obtained in the CRC analysis of the data, are listed in table 3.

In fig. 6, the curves show the CRC calculations for the $^{14}\mathrm{C}+{}^{11}\mathrm{B}$ potential scattering (curve ⟨pot⟩), reorientation of ^{11}B (curve ⟨reor⟩) and transfers of t-cluster (curve ⟨t⟩), sequential transfers of protons and neutrons (curves ⟨nn⟩ and ⟨pp⟩, respectively), n + d and d + n (curve ⟨nd⟩, coherent sum), p + α and α + p (curve ⟨pα >). Σ- and ⟨tr⟩-curves show the coherent sums of all processes and transfer reactions, respectively.

As fig. 6 shows, the potential scattering dominates for $\theta_{\mathrm{c.m.}} < 120°$. The ^{11}B ground-state spin reorientation is important at large angles and the transfer reactions only give a small contribution to the elastic scattering channel.

Table 2. Spectroscopic amplitudes S_x of x-clusters in the $A = C + x$ systems.

A	C	x	nL_j	S_x	A	C	x	nL_j	S_x
^{11}B	^{10}Be	p	$1P_{3/2}$	0.699	^{12}C	^{11}B$^*_{2.125}$	p	$1P_{1/2}$	$-1.206^{(a)}$
^{11}B$^*_{2.125}$	^{10}Be	p	$1P_{1/2}$	0.699	^{12}C	^{11}B$^*_{5.021}$	p	$1P_{3/2}$	$-1.706^{(a)}$
^{11}B$^*_{5.021}$	^{10}Be	p	$1P_{3/2}$	0.699	^{12}C	^{11}B$^*_{6.793}$	p	$1P_{1/2}$	$-1.206^{(a)}$
^{11}B$^*_{8.559}$	^{10}Be	p	$1P_{3/2}$	0.699	^{12}C	^{11}B$^*_{8.559}$	p	$1P_{3/2}$	$-1.706^{(a)}$
^{11}B	^{10}B	n	$1P_{3/2}$	$-1.347^{(a)}$	^{13}C	^{11}B	d	$2S_1$	-0.263
^{11}B$^*_{4.445}$	^{10}B	n	$1P_{1/2}$	$0.152^{(a)}$				$1D_1$	-0.162
			$1P_{3/2}$	0.271				$1D_2$	$-0.485^{(a)}$
^{11}B$^*_{5.021}$	^{10}B	n	$1P_{3/2}$	$-1.347^{(a)}$	^{13}C	^{11}B$^*_{2.125}$	d	$2S_1$	$0.093^{(a)}$
^{11}B$^*_{8.559}$	^{10}B	n	$1P_{3/2}$	$-1.347^{(a)}$				$1D_1$	$-0.457^{(a)}$
^{12}B	^{11}B	n	$1P_{1/2}$	$-0.142^{(a)}$	^{13}C	^{11}B$^*_{4.445}$	d	$1D_2$	-0.111
			$1P_{3/2}$	-0.127				$1D_3$	$-0.417^{(a)}$
^{12}B	^{11}B$^*_{2.125}$	n	$1P_{1/2}$	0.402	^{13}C	^{11}B$^*_{5.021}$	d	$2S_1$	-0.263
			$1P_{3/2}$	$0.142^{(a)}$				$1D_1$	-0.162
^{12}B	^{11}B$^*_{4.445}$	n	$1P_{3/2}$	$0.147^{(a)}$				$1D_2$	$-0.485^{(a)}$
^{12}B	^{11}B$^*_{5.021}$	n	$1P_{1/2}$	$-0.142^{(a)}$	^{14}C	^{10}Be	α	$3S_0$	-0.556
			$1P_{3/2}$	-0.127	^{14}C	^{11}B	t	$2P_{3/2}$	$-0.368^{(a)}$
^{12}B	^{11}B$^*_{8.559}$	n	$1P_{1/2}$	$-0.142^{(a)}$	^{14}C	^{11}B$^*_{2.125}$	t	$2P_{1/2}$	$-0.261^{(a)}$
			$1P_{3/2}$	-0.127	^{14}C	^{11}B$^*_{4.445}$	t	$1F_{3/2}$	-1.105
^{13}B	^{11}B	^{2}n	$2S_0$	0.623	^{14}C	^{11}B$^*_{5.021}$	t	$2P_{3/2}$	$-0.368^{(a)}$
			$1D_2$	0.197	^{14}C	^{12}B	d	$1D_1$	-1.010
^{13}B	^{11}B$^*_{2.125}$	^{2}n	$1D_2$	$0.197^{(a)}$	^{14}C	^{13}B	p	$1P_{3/2}$	$1.695^{(a)}$
			$1D_2$	0.197	^{14}C	^{12}C	^{2}n	$2S_0$	0.615
^{13}B	^{11}B$^*_{4.445}$	^{2}n	$1D_2$	$0.394^{(a)}$	^{14}C	^{13}C	n	$1P_{1/2}$	$-1.094^{(a)}$
^{13}B	^{11}B$^*_{5.021}$	^{2}n	$2S_0$	0.623	^{15}C	^{14}C	n	$2S_{1/2}$	-0.882
			$1D_2$	0.197	^{15}N	^{11}B	α	$2D_2$	$0.435^{(a)}$
^{13}B	^{11}B$^*_{6.743}$	^{2}n	$1D_2$	0.965	^{15}N	^{11}B$^*_{2.125}$	α	$3S_0$	$-0.465^{(a)}$
^{13}B	^{11}B$^*_{8.559}$	^{2}n	$2S_0$	0.623	^{15}N	^{11}B$^*_{4.445}$	α	$2D_2$	-0.465
			$1D_2$	0.197	^{15}N	^{11}B$^*_{5.021}$	α	$2D_2$	$-0.435^{(a)}$
^{12}C	^{11}B	p	$1P_{3/2}$	$-1.706^{(a)}$	^{15}N	^{14}C	p	$1P_{1/2}$	-0.598

(a) $S_{\text{FRESCO}} = (-1)^{J_C+j-J_A} S_x = -S_x$.

Table 3. Parameters of the nucleus-nucleus potentials.

Nuclear system	Sets	$E_{\text{c.m.}}$ (MeV)	V_0 (MeV)	r_V (fm)	a_V (fm)	W_S (MeV)	r_W (fm)	a_W (fm)	J_V (MeV fm^2)	J_W (MeV fm^2)	R_V (fm)	R_W (fm)	Ref.
^{12}C+^{11}B	A	25.57	241.6	0.788	0.670	9.0	1.250	0.670	466	58	3.71	5.03	[3]
^{13}C+^{11}B	B	24.38	256.7	0.788	0.740	8.0	1.250	0.740	499	51	3.92	5.22	[4]
^{14}C + ^{11}B	C	25.20	266.6	0.750	0.740	7.5	1.345	0.740	441	56	3.85	5.56	
^{14}C + ^{11}B$^*_{5.021}$	C_1	20.18	266.6	0.750	0.740	4.5	1.330	0.700	441	32	3.85	5.44	
^{14}C + ^{11}B$^*_{7.978}$	C_2	17.23	266.6	0.750	0.740	4.5	1.345	0.740	441	34	3.85	5.56	
^{14}C + ^{11}B$^*_{8.560}$	C_3	17.23	266.6	0.750	0.740	6.5	1.345	0.740	441	49	3.85	5.56	

3.2 Inelastic scattering

The measured angular distributions of ^{14}C + ^{11}B inelastic scattering for the transitions to the excited states of ^{11}B are shown in figs. 7–9.

Figure 7 shows the angular distributions for the transitions to 2.125 MeV ($1/2^-$), 4.445 MeV ($5/2^-$) and 5.021 MeV ($3/2^-$) excited states of ^{11}B. The dashed curves $\langle$inel$\rangle$ and $\langle$tr$\rangle$ show the CRC calculations for the collective excitations and reaction transfers, respectively. Σ-curves present the coherent sums of both types of excitation. As one can see, the collective excitations dominate in all transitions. Figure 8 shows the measured summary angular distribution of the ^{14}C + ^{11}B inelastic scattering at the energy $E_{\text{lab}}(^{11}\text{B}) = 45$ MeV for the transitions to the unresolved 6.743 MeV ($7/2^-$) and 6.792 MeV ($1/2^+$) excited states of ^{11}B and the 6.728 MeV (3^-) state of ^{14}C. The dashed curves show the CRC calculations for the individual collective excitations of ^{11}B and ^{14}C. The Σ-curve presents the incoherent sum of the individual transitions.

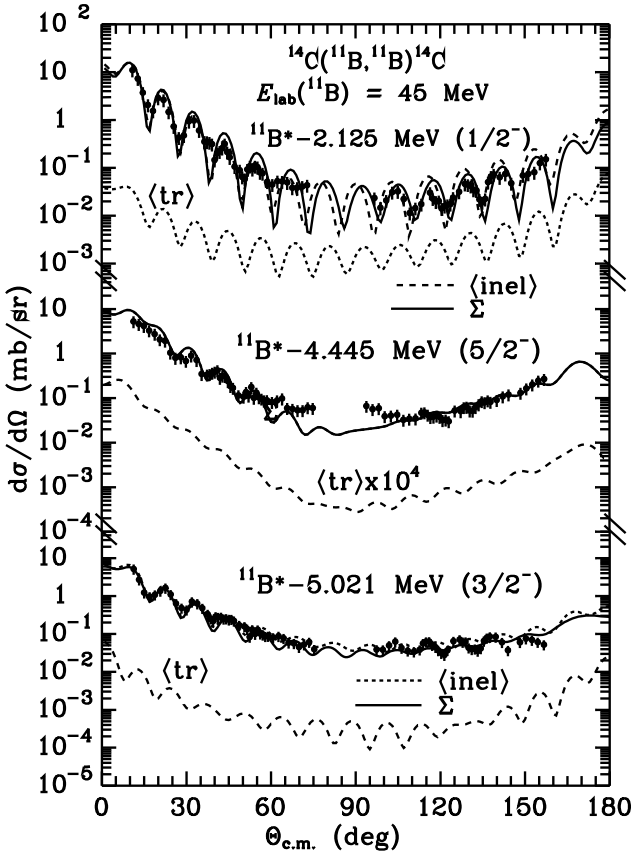

Fig. 7. Angular distributions of the $^{14}C + ^{11}B$ inelastic scattering at the energy $E_{lab}(^{11}B) = 45$ MeV for the transitions to the 2.125 MeV $(1/2^-)$, 4.445 MeV $(5/2^-)$ and 5.025 MeV $(3/2^-)$ excited states of ^{11}B. The curves show the CRC calculations.

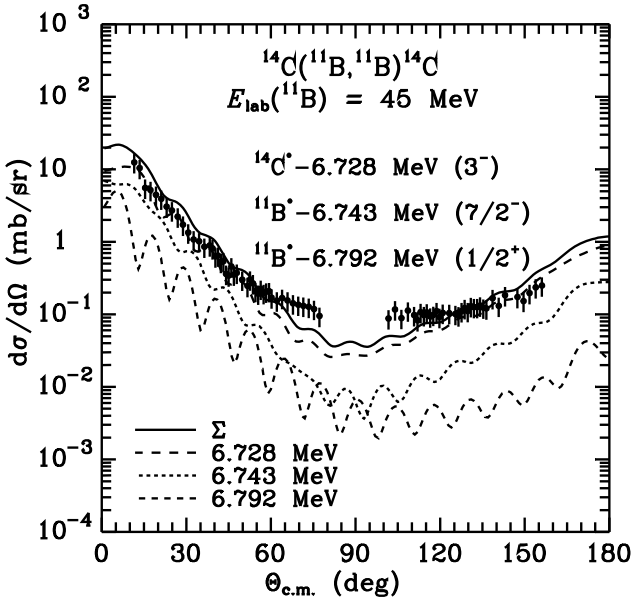

Fig. 8. Angular distributions of the $^{14}C + ^{11}B$ inelastic scattering at the energy $E_{lab}(^{11}B) = 45$ MeV for the transitions to the 6.743 MeV $(7/2^-)$, 6.792 MeV $(1/2^+)$ excited states of ^{11}B and 6.728 MeV (3^-) state of ^{14}C. The curves show the CRC calculations.

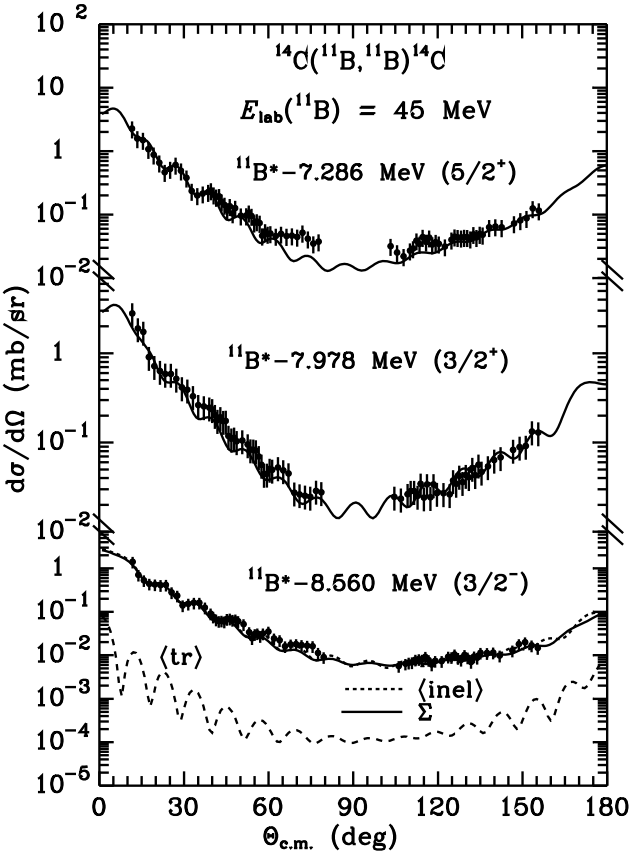

Fig. 9. Angular distributions of the $^{14}C + ^{11}B$ inelastic scattering at the energy $E_{lab}(^{11}B) = 45$ MeV for the transitions to the 7.286 MeV $(5/2^+)$, 7.978 MeV $(3/2^+)$ and 8.560 MeV $(3/2^-)$ excited states of ^{11}B. The curves show the CRC calculations.

As one can see, the transition to the 6.728 MeV (3^-) excited state of ^{14}C dominates.

The measured angular distributions of the $^{14}C + ^{11}B$ inelastic scattering at the energy $E_{lab}(^{11}B) = 45$ MeV for the transitions to the 7.286 MeV $(5/2^+)$, 7.978 MeV $(3/2^+)$ and 8.56 MeV $(3/2^-)$ excited states of ^{11}B are presented in fig. 9. The curves show the CRC calculations for the collective transitions to the excited states of ^{11}B. As a typical example, the curve ⟨tr⟩ shows the CRC calculation for the coherent sum of all transfer reactions studied here. One can see that the transfer reactions contributions are small to the CRC calculation for this inelastic scattering channel. The same is observed for other excited states of ^{11}B.

3.3 Comparison of the $^{12,13,14}C + ^{11}B$ potentials

First, it is interesting to compare the deduced $^{14}C + ^{11}B$ Woods-Saxon real potential with a double folding potential, which was calculated using the M3Y (Reid) nucleon-nucleon potential and charge distributions in ^{11}B and ^{14}C [12]. The calculation was performed with the code DFPOT [13,14].

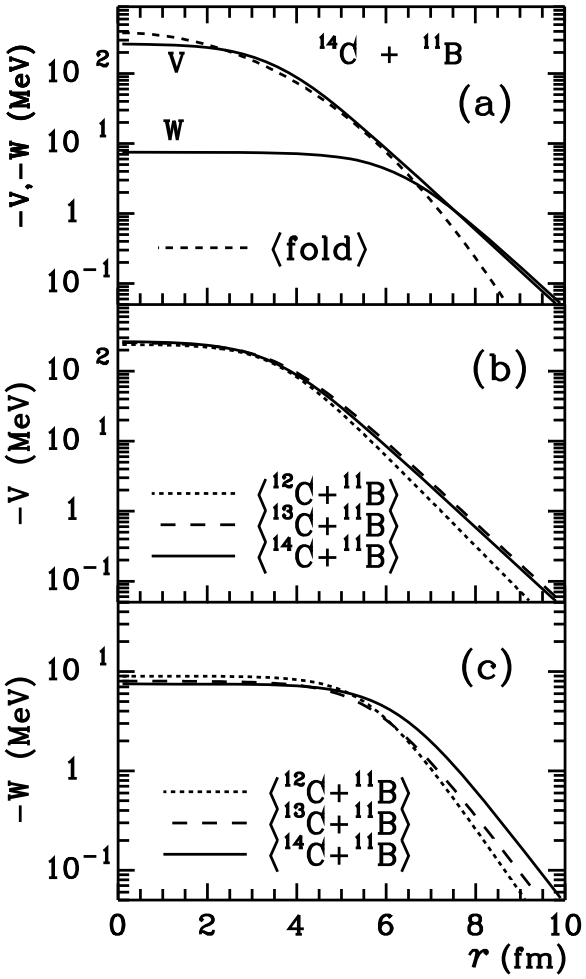

Fig. 10. Optical potentials for the $^{13,14}\mathrm{C} + {}^{11}\mathrm{B}$ interactions at the energy $E_{\mathrm{lab}}(^{11}\mathrm{B}) = 45\,\mathrm{MeV}$ and for the $^{12}\mathrm{C} + {}^{11}\mathrm{B}$ interaction at $E_{\mathrm{lab}}(^{11}\mathrm{B}) = 49\,\mathrm{MeV}$. Curve ⟨fold⟩ (a) shows the $^{14}\mathrm{C} + {}^{11}\mathrm{B}$ double-folding potential.

The deduced ^{14}C+^{11}B potential is compared with their double-folding potential in fig. 10(a). As one can see, the real part of the deduced $^{14}\mathrm{C} + {}^{11}\mathrm{B}$ potential is in a good agreement with the folding potential in the peripheral region, where nuclear processes take place.

Comparisons of the imaginary and real parts of the $^{14}\mathrm{C} + {}^{11}\mathrm{B}$ potential with that of $^{12,13}\mathrm{C} + {}^{11}\mathrm{B}$ [3,4] are shown in figs. 10(b) and (c). One can see that these potentials differ mainly by their imaginary parts.

How these differences affect the angular distribution of the $^{14}\mathrm{C} + {}^{11}\mathrm{B}$ elastic scattering, can be seen in fig. 11, where the curves ⟨A⟩, ⟨B⟩ and ⟨C⟩ show the CRC calculations with the potential parameters of the $^{12}\mathrm{C} + {}^{11}\mathrm{B}$, $^{13}\mathrm{C} + {}^{11}\mathrm{B}$ and $^{14}\mathrm{C} + {}^{11}\mathrm{B}$ elastic scattering, respectively. Figure 11 shows that there is great sensitivity in the angular distribution to small isotopic differences of the $^{12,13,14}\mathrm{C} + {}^{11}\mathrm{B}$ potential parameters.

4 Summary and conclusions

New experimental data for the $^{14}\mathrm{C} + {}^{11}\mathrm{B}$ inelastic scattering at the energy $E_{\mathrm{lab}}(^{11}\mathrm{B}) = 45\,\mathrm{MeV}$ were measured

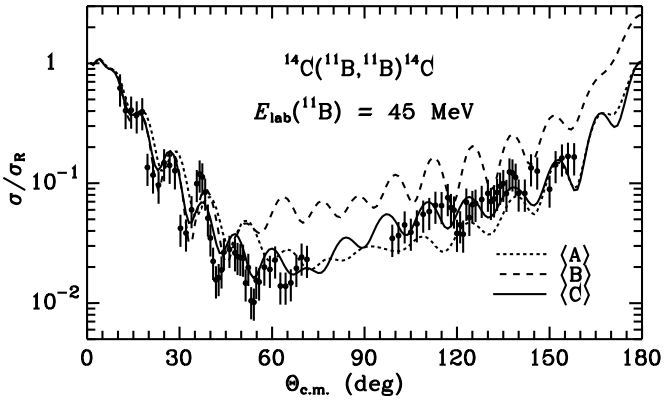

Fig. 11. Angular distributions of the $^{14}\mathrm{C} + {}^{11}\mathrm{B}$ elastic scattering at the energy $E_{\mathrm{lab}}(^{11}\mathrm{B}) = 45\,\mathrm{MeV}$. The curves show the CRC calculations using $^{12}\mathrm{C} + {}^{11}\mathrm{B}$, $^{13}\mathrm{C} + {}^{11}\mathrm{B}$ and $^{14}\mathrm{C} + {}^{11}\mathrm{B}$ potential parameters (curves ⟨A⟩, ⟨B⟩ and ⟨C⟩, respectively).

for transitions of ^{11}B to its excited states from 2.125 to 8.56 MeV. Experimental data for the $^{14}\mathrm{C}+{}^{11}\mathrm{B}$ elastic and inelastic scattering were analyzed within the OM and CRC method. In the CRC analysis of the data, the $^{14}\mathrm{C} + {}^{11}\mathrm{B}$ elastic and inelastic scattering, spin reorientation of ^{11}B as well as one- and two-step transfer reactions were included in the coupling-channels scheme. The low-energy excited states of ^{11}B and ^{14}C were assumed to have a collective nature (rotation and vibration).

The $^{14}\mathrm{C}+{}^{11}\mathrm{B}$ potential parameters were deduced and compared with that of the $^{12,13}\mathrm{C} + {}^{11}\mathrm{B}$ interactions. The main difference for ^{11}B elastic scattering from the various carbon isotopes was in the deduced imaginary potentials, with that for ^{14}C being greater than those for ^{12,13}C, as could be predicted based on the differences in the magnitude of their large angle scattering. This comparison shows the importance of measuring large angle scattering when possible.

Collective excitations dominate the ^{11}B inelastic scattering, and the presently deduced deformations are consistent with those found previously for its inelastic scattering in light interacting nuclear systems and for the heavier system $^{11}\mathrm{B} + {}^{40}\mathrm{Ca}$ [15].

References

1. J.S. Blair, Phys. Rev. **115**, 928 (1959).
2. L.A. Parks, K.W. Kemper, A.H. Lumpkin *et al.*, Phys. Lett. B **70**, 27 (1977).
3. A.T. Rudchik, A. Budzanowski, V.K. Chernievsky *et al.*, Nucl. Phys. A **695**, 51 (2001).
4. S.Yu. Mezhevych, K. Rusek, A.T. Rudchik *et al.*, Nucl. Phys. A **724**, 29 (2003).
5. S.Yu. Mezhevych, A.T. Rudchik, K. Rusek *et al.*, Nucl. Phys. A **753**, 13 (2005).
6. M. Kowalczyk, *SMAN: A Code for Nuclear Experiments*, Warsaw University report (1998) unpublished.
7. Yu.F. Smirnov, Yu.M. Tchuvil'sky, Phys. Rev. C **15**, 84 (1977).

8. A.T. Rudchik, Yu.M. Tchuvil'sky, *The code DESNA*, The Kiev Institute for Nuclear Researches report KIYAI-82-12 (1982).
9. A.T. Rudchik, Yu. M. Tchuvil'sky, Ukr. Fiz. Zh. **30**, 819 (1985).
10. B.S. Nilsson, *SPI-GENOA: An Optical Model Search Code*, Niels Bohr Institute report (1976).
11. I.J. Thompson, Comput. Phys. Rep. **7**, 167 (1988).
12. H. De Vries, C.W. De Jager, C. De Vries, At. Data Nucl. Data Tables **36**, 495 (1987).
13. J. Cook, Comput. Phys. Commun. **25**, 125 (1982).
14. J. Cook, Comput. Phys. Commun. **35**, 775 (1984).
15. V. Hnizdo, C.W. Glover, K.W. Kemper, Phys. Rev. C **23**, 236 (1981).